The role of dry intrusions in breaks of the Indian summer monsoon

Deoras, A. ORCID: https://orcid.org/0009-0006-5407-6520, Turner, A. G. ORCID: https://orcid.org/0000-0002-0642-6876, Volonté, A. ORCID: https://orcid.org/0000-0003-0278-952X, Schiemann, R. K. H. ORCID: https://orcid.org/0000-0003-3095-9856, Wilcox, L. J. ORCID: https://orcid.org/0000-0001-5691-1493 and Menon, A. ORCID: https://orcid.org/0000-0001-9347-0578 (2026) The role of dry intrusions in breaks of the Indian summer monsoon. Journal of Climate, 39 (5). pp. 1237-1250. ISSN 1520-0442 doi: 10.1175/JCLI-D-25-0004.1 Available at https://centaur.reading.ac.uk/127873/

The Role of Dry Intrusions in Breaks of the Indian Summer Monsoon

AKSHAY DEORAS,[a,b] ANDREW G. TURNER,[a,b] AMBROGIO VOLONTÉ,[a,b] REINHARD K. H. SCHIEMANN,[a] LAURA J. WILCOX,[a] AND ARATHY MENON[c]

[a] *National Centre for Atmospheric Science, University of Reading, Reading, United Kingdom*
[b] *Department of Meteorology, University of Reading, Reading, United Kingdom*
[c] *Met Office, Exeter, United Kingdom*

(Manuscript received 2 January 2025, in final form 11 November 2025, accepted 11 January 2026)

ABSTRACT: The Indian summer monsoon (ISM) is crucial to over a billion people since it supplies over 75% of the country's annual precipitation. Significant intraseasonal variability in rainfall affects people, with breaks responsible for causing water shortages. It is known that dry intrusions play a role in breaks; however, it is not well understood compared to their role during progressions of the onset and withdrawal of the ISM. In this study, we use observations and the fifth generation ECMWF atmospheric reanalysis (ERA5) to understand the role of dry intrusions in breaks during 1940–2023. We develop an index based on moisture deficit to identify dry intrusions and find that most breaks are associated with dry intrusions emanating from arid regions to the west and northwest of India. These dry intrusions begin to enter India around a week prior to the middle day of breaks, reaching their peak strength over northwest India and adjoining eastern Pakistan 2–3 days prior to the middle day of breaks. Vertical profiles reveal that these are midlevel dry intrusions, which are similar to those driving the direction of the withdrawal of the ISM. As breaks evolve, these dry intrusions deepen throughout their horizontal extent and descend into the country, stabilizing the troposphere and creating an unfavorable environment for deep convection. We also find that extended breaks have stronger dry intrusions as precursors. Thus, this work helps establish a causal relationship between midlevel dry intrusions and breaks. The results could help improve forecasts of breaks, ultimately benefiting stakeholders in improving long-term planning.

KEYWORDS: Deep convection; Dry intrusions; Trajectories; Monsoons; Intraseasonal variability; Tropical variability

1. Introduction

The Indian summer monsoon (hereafter the monsoon) supplies more than 75% of India's annual precipitation between June and September (e.g., Parthasarathy and Mooley 1978), providing water that is important for summer crops, hydroelectric power generation, groundwater recharge, and basic human needs. The monsoon exhibits variability across a broad range of time scales, of which subseasonal fluctuations between wet and dry spells (hereafter breaks) have a huge impact on rain-fed agriculture and other users of water resources. This is because seasonal monsoon rainfall is correlated with the durations of wet spells and breaks (Gadgil and Joseph 2003). A series of consecutive breaks often leads to a drought, and severe droughts can reduce the gross domestic product (GDP) of the country by 2%–5% (Gadgil 2006). For example, the two severe breaks during July 2002 led to a strong monthly rainfall deficit of around 50% (Bhat 2006), which triggered a severe drought and reduced GDP by over 2% (Gadgil 2006). While breaks typically last for 3–5 days (e.g., Ramamurthy 1969), some last even longer and cause a more severe impact, such as the extended break of 17 days during the 1972 monsoon season (Pai et al. 2016; Chuphal et al. 2024). Accurate forecasting of breaks is therefore important for over a billion people, for which it is necessary to understand their precursors.

Synoptic features associated with breaks were first examined by Blanford (1886), who observed that the monsoon trough shifts northward to the Himalayan foothills, reducing precipitation over central India. A number of studies have analyzed synoptic features and precipitation patterns of breaks since then (e.g., Ramamurthy 1969; Raghavan 1973; Rao 1976; Krishnan et al. 2000; De and Mukhopadhyay 2002; Gadgil and Joseph 2003; Bhatla et al. 2004; Joseph and Sijikumar 2004; Pai et al. 2014). The consensus among these studies is that the weakening of monsoon winds during breaks reduces the moisture transport toward most of India, and easterly low-level monsoon winds over northern India are replaced by westerlies or northwesterlies that are relatively dry. At upper levels, the Tibetan anticyclone shifts eastward of its normal position, allowing southward penetrating troughs to bring dry extratropical air into India (Ramaswamy 1962). As a result, most of the country experiences suppressed precipitation, except for the southeast coast and the Himalayan foothills.

It is known that modes of tropical intraseasonal variability modulate the occurrence of breaks. Pai et al. (2011) found that about 83% of total breaks during 1974–2008 occurred during phases 1–2 and 7–8 of the Madden–Julian oscillation

Denotes content that is immediately available upon publication as open access.

Supplemental information related to this paper is available at the Journals Online website: https://doi.org/10.1175/JCLI-D-25-0004.s1.

Corresponding author: Akshay Deoras, akshay.deoras@reading.ac.uk

DOI: 10.1175/JCLI-D-25-0004.1

(MJO), when convection was enhanced over the western equatorial Indian Ocean and western Pacific, respectively. In fact, most breaks occurred during MJO phase 1. While the eastward-propagating MJO is the dominant mode of the tropical intraseasonal variability in boreal winter, the boreal summer intraseasonal oscillation (BSISO) prevails in boreal summer (e.g., Wang and Xie 1997). Kikuchi (2021) found that most breaks during 1979–2007 occurred during BSISO phases 1–2 and 8, when convection was suppressed over most of India.

Pisharoty and Asnani (1960) found that the midlevel subtropical anticyclone over the Sahara Desert and Arabian Sea extends into India prior to the onset of breaks. Krishnamurti et al. (2010) also observed the presence of this anticyclone over the western Arabian Peninsula between 700 and 300 hPa 3 days prior to the onset of breaks. While they argued that the northward extension of the intertropical convergence zone and a strong local Hadley cell over North Africa play an important role in the development of the anticyclone, Samanta et al. (2016) attributed its formation to Rossby wave breaking over West Asia that transports high potential vorticity air from the subtropical jet stream. Both studies have shown that dry intrusions from West Asia descend around the anticyclone, transporting very dry upper-tropospheric air to the Arabian Sea and central India. Krishnamurti et al. (2010) performed a back-trajectory analysis to understand how airmass properties during breaks differ from those during wet spells. They found that the air terminating at 700 hPa over central India during breaks originated in West Asia and was dry, whereas the air terminating between the surface and 850 hPa was moist and of oceanic origin. In contrast, the air terminating between the surface and midlevels during wet spells was mostly of oceanic origin. They concluded that the midlevel dry air over central India inhibited the development of deep convection, triggering breaks. These results agree with Bhat (2006), who also observed an advection of dry air from deserts in the Middle East over the Arabian Sea during the July 2002 break. The dry air caused strong atmospheric inversions around 800 hPa, preventing the occurrence of deep convection in the region. Boos and Hurley (2013) pointed at the role of terrain gaps between mountain ranges in allowing this dry air to flow from the deserts in western Asia toward the monsoon region, as their analysis of climate models suggests that negative biases in surface moist static energy (MSE) are related to an excessively smoothed representation of the topography to the west of the Tibetan Plateau, including of the Hindu Kush mountain range.

Using reanalysis and coupled model ensemble simulations, Prasanna and Annamalai (2012) conducted moisture and MSE budget analyses to diagnose the moist processes governing breaks. They found that the advection of dry air from northern to central India begins about 15 days prior to the onset of negative rainfall anomalies. This advection is driven by anticyclonic circulation anomalies that are forced by suppressed convection over the equatorial Indian Ocean. Additionally, enhanced rainfall over the tropical western Pacific triggers a Rossby wave response, which further transports low MSE air southward into central India. Once a break is initiated, enhanced radiative cooling amplifies low-level divergence and suppresses rainfall over central India. This cooling, contrasted with enhanced radiative warming over the equatorial Indian Ocean, helps anchor a local Hadley circulation with subsidence over central India, reinforcing the dry conditions.

Singh and Sandeep (2022) further examined the role of dry intrusions in 38 breaks that occurred between 1981 and 2014. They identified dry intrusions by measuring the zonal moisture deficit transport between 950 and 300 hPa, for which they considered a meridional transect across northwestern India and adjoining eastern Pakistan. They concluded that most breaks in this period were associated with dry intrusions and that the monsoon low-level jet transported dry air from the western and northern Arabian Sea to northern and central India. In a more recent study, Singh and Sandeep (2024) considered a small box (21°–24°N, 70°–75°E) and observed strong dry intrusions at 850 hPa over the northern Arabian Sea from nearby arid regions around 4 days prior to the onset of breaks during 1981–2019. Following the onset of breaks, these dry intrusions strengthened and entered northwestern India and suppressed deep convection. They began to weaken after a further 4 days. While these studies demonstrate the role of dry intrusions in breaks, they have some limitations. First, the analysis of zonal moisture deficit transport in Singh and Sandeep (2022) and the choice of a single pressure level (i.e., 850 hPa) in Singh and Sandeep (2024) do not help in truly identifying the origins of the (primarily northwesterly) dry air, other than its immediate position adjacent to India. This issue is exacerbated by the box used in Singh and Sandeep (2024) being too small and located too far south to capture the core of the dry air. Second, the sample size considered in previous studies is small; for example, Bhat (2006) analyzed only a single monsoon season, Krishnamurti et al. (2010) looked at a handful of break and active events, whereas Singh and Sandeep (2022) analyzed 38 breaks. Thus, a few questions arise that warrant a further investigation into the role of dry intrusions in breaks. First, what is the causal relationship between dry intrusions and breaks? This is an important question that will help understand how breaks interact with dry intrusions. Second, what is the preferred direction of dry intrusions into India? This question arises since the results of Rai and Raveh-Rubin (2023) suggest that dry intrusions impacting India can also originate in the midlatitudes of the Southern Hemisphere, a hypothesis already formulated by Rodwell (1997). Third, are these dry intrusions similar to those modulating progressions of the onset (Parker et al. 2016) and withdrawal of the monsoon (Deoras et al. 2024)? Last, do dry intrusions play a role in enhancing the duration of breaks? In this study, we attempt to answer these questions by analyzing a climatology of dry intrusions and breaks.

We present an outline of the data and methodology in section 2 and explore characteristics of dry intrusions and their relationship with breaks in section 3. We then look at the kinematics and thermodynamics of dry intrusions in sections 4 and 5, respectively. We evaluate the relationship between the strength of dry intrusions and the duration of breaks in section 6 and finally conclude in section 7.

2. Methodology and data

a. ERA5 reanalysis

We use data from the fifth generation European Centre for Medium-Range Weather Forecasts atmospheric reanalysis (ERA5; Hersbach et al. 2020) to create a catalogue of dry intrusions, compute Lagrangian trajectories, and analyze thermodynamic fields. ERA5 data are available globally from 1940 at an hourly temporal resolution and on a 0.25° × 0.25° grid. The back extension of the ERA5 final release data from 1959 to 1940 was made publicly available since March 2023. The back-extension period belongs to the presatellite era, when in situ observations were limited, whereas upper-air data were not available before the mid-1940s (Hersbach 2023). Deoras et al. (2024) assessed the suitability of using data from ERA5 back to 1940 by comparing the behavior of the monsoon circulation and thermodynamic fields between 1940 and 1958 and 1959–2022. They concluded that the ERA5 reanalysis is reliable in this period, so we consider the period between 1940 and 2023 in this study. We also use ERA5 as an alternative source of precipitation dataset for verifying our results. Mahto and Mishra (2019) compared ERA5 precipitation with the Climate Forecast System Reanalysis, ERA-Interim, Modern-Era Retrospective Analysis for Research and Applications, version 2, and Japanese 55-year Reanalysis datasets and found that ERA5 outperformed other reanalyses for monsoon precipitation. All variables considered in this study are instantaneous, except for precipitation that is accumulated hourly.

b. IMD gridded precipitation dataset

We use the fourth version of the daily gridded precipitation dataset from the India Meteorological Department (IMD; Pai et al. 2014), which is available from 1901 at a spatial resolution of 0.25° × 0.25°. It uses data from rain gauge stations across India, whose number has varied in time from about 1450 in 1901 to about 3950 during the period 1991–94. On an average, daily data from about 2600 rain gauge stations were available over the last century (Pai et al. 2014). The gauge data are regridded using a simple inverse distance weighted interpolation method (Shepard 1968). While the spatial distribution of monsoon rainfall is well captured in the dataset in general, the low spatial density of rain gauges in mountainous regions of northern and northeastern India makes it less reliable there (Pai et al. 2014). Given that this dataset is based on Indian rain gauges, it is available only for mainland India.

c. Vertically integrated moisture deficit flux

To identify dry intrusions, we develop an index that measures the moisture deficit flux in the troposphere. Its vertical integral, which we name "the vertically integrated moisture deficit flux (VIMDF)," is calculated as follows:

$$\mathrm{VIMDF} = \frac{1}{g}\int \mathbf{u}(q_s - q)dp, \tag{1}$$

where $\mathbf{u}$ is the horizontal wind vector, q_s is the saturation specific humidity, q is the specific humidity, and other symbols have their usual meanings. A key difference between the VIMDF and the index developed by Singh and Sandeep (2022) is that the former measures the horizontal flux of the moisture deficit, whereas the latter measures only the zonal flux of the moisture deficit. As discussed in section 1, Singh and Sandeep (2022) considered pressure levels between 950 and 300 hPa to identify dry intrusions, whereas Krishnamurti et al. (2010) analyzed pressure levels between 700 and 300 hPa. We speculate that by excluding pressure levels between 850 and 700 hPa, we might miss detecting dry intrusions that occurred at low levels, such as those observed during the July 2002 break (Bhat 2006). We therefore test the sensitivity of the VIMDF index by integrating it from 700 to 300 hPa and from 850 to 300 hPa. Parker et al. (2016) have shown that a wedge of midtropospheric dry air, which emanates from the midlatitudes, is present over India during the premonsoon season. It gradually retreats toward the northwest as the monsoon onset progresses. So, we will test if the VIMDF index detects the retreat of this dry air, for which we analyze VIMDF composites centered on 15 May, 15 June, and 15 July 1940–2023 (Fig. 1). The presence of the climatological dry air to the north of 20°N is indicated by the large magnitude of the VIMDF, and the dry air weakens as the monsoon onset progresses. The VIMDF increases when pressure levels between 850 and 700 hPa are considered (Figs. 1d–f). We therefore integrate the VIMDF between 850 and 300 hPa in the remainder of this study. We calculate VIMDF anomalies against a daily climatology during June–September 1940–2023. Thus, if the magnitude of the VIMDF anomaly is positive, it indicates that the moisture deficit is larger than the climatology (i.e., the presence of anomalous dry air).

Singh and Sandeep (2024) considered a domain encompassing western India (21°–30°N, 70°–80°E) to analyze dry intrusions. Given that most of the dry air enters India through regions to its northwest (see Fig. 3f), we select a domain (26°–32°N, 64°–70°E; shown as a blue box in Fig. 1a) that encompasses a larger area in northwestern India and adjoining eastern Pakistan compared to the domain considered by Singh and Sandeep (2024). This domain reflects the location of maximum VIMDF anomalies and also aligns with a ridge in trajectory density extending northwest, as shown in Fig. 6b. We name this domain the northwest domain for brevity.

d. Identification of monsoon breaks

We use the IMD gridded dataset to identify breaks during June–September 1940–2023,[1] for which we follow the method proposed by Rajeevan et al. (2010). An event is classified as a

[1] We note that breaks occurring during June and September are generally ignored to prevent contamination of the results by progressions of the onset and withdrawal of the monsoon. However, we do not eliminate such breaks in this study since our objective is to analyse the climatology of breaks and dry intrusions irrespective of the month of occurrence. Furthermore, the occurrence of dry intrusions over India is not confined to July and August (Parker et al. 2016; Deoras et al. 2024). Thus, the exclusion of breaks occurring during June and September is not necessitated for this study.

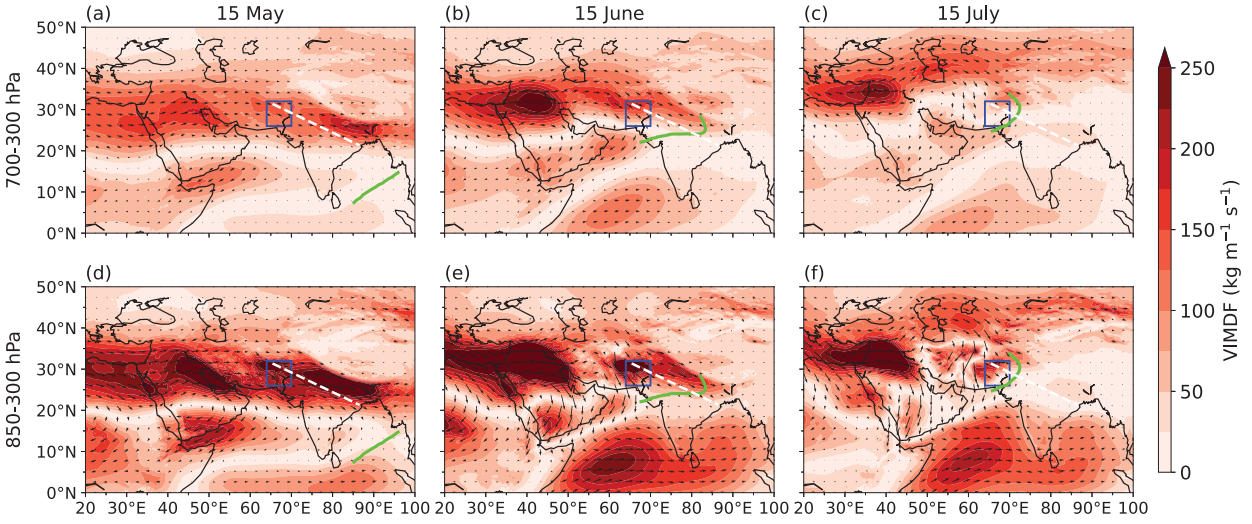

FIG. 1. Pentad-mean VIMDF (kg m^{-1} s^{-1}) centered on (a),(d) 15 May, (b),(e) 15 Jun, and (c),(f) 15 Jul over 1940–2023. VIMDF is integrated from (a)–(c) 700 to 300 hPa and from (d)–(f) 850 to 300 hPa. The blue box in all subplots shows the northwest domain (26°–32°N, 64°–70°E) considered for further analysis of the VIMDF. A white dashed line in (a) shows a transect used for computing vertical cross sections of equivalent potential temperature. Solid green lines show climatological isochrones of the monsoon onset on these dates as defined by the IMD.

break if the standardized precipitation anomaly over the core monsoon zone (shown in magenta in Fig. 2a) is less than −1 for at least three consecutive days. A total of 188 breaks are identified, and the spatial distribution of precipitation and precipitation anomaly during breaks is shown in Figs. 2a and 2b, respectively. The mean duration of breaks is 5.5 days, and most of them have a duration of 3–4 days (Fig. 2c). Most breaks occur in August, which is followed by July, September, and June (not shown). We then identify the middle day of each break, which depends on whether the duration of breaks is an even or odd number. For example, if the duration of a break is 5 days, the middle day is selected as the third day from the onset of the break. If the duration of a break is 4 days, either the second or the third day is selected depending on which of the two gets the least precipitation over the core monsoon zone.

We also identify breaks using the ERA5 reanalysis to test the sensitivity of our results to the choice of the precipitation dataset. One hundred ninety-eight breaks are identified during June–September 1940–2023, and their mean duration is 5.7 days. Figures S1a and S1b in the online supplemental material show precipitation and anomalous precipitation, respectively. The spatial pattern of precipitation and its anomaly during breaks in the two datasets is similar, except for the southeastern part of the core zone, where the magnitude of precipitation in the IMD gridded dataset is larger than in ERA5. The frequency distribution of the duration of breaks identified in ERA5 (Fig. S1c) is similar to that in the IMD gridded dataset, and breaks featuring a duration of 3–4 days are most common in both datasets.

e. *Lagrangian trajectories*

Lagrangian trajectories are a powerful tool for airmass analysis since they can be used to identify the origin of air masses and understand how they evolve in space and time. In this study, we compute Lagrangian trajectories using the Lagrangian analysis tool LAGRANTO (Sprenger and Wernli 2015),

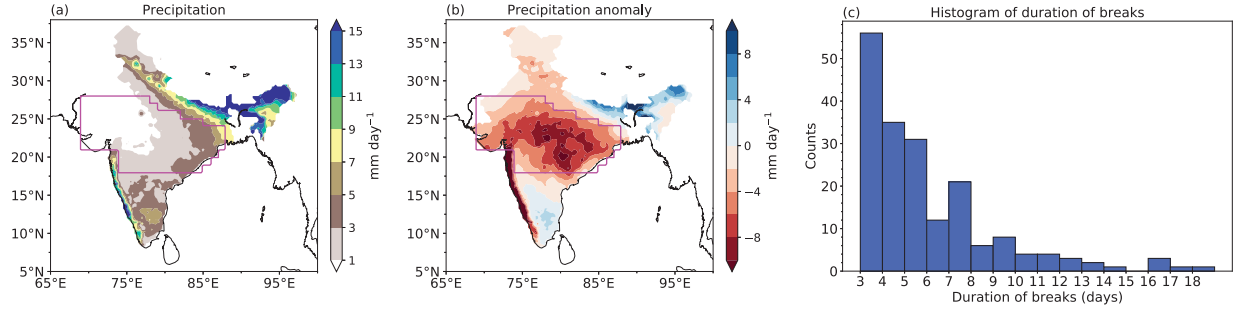

FIG. 2. (a) Daily mean precipitation (mm day^{-1}) and (b) precipitation anomaly (mm day^{-1}) during 188 monsoon breaks. The anomaly is computed against a daily climatology during 1940–2023. (c) A histogram of the duration of 188 breaks. The core monsoon zone is highlighted in magenta in (a) and (b).

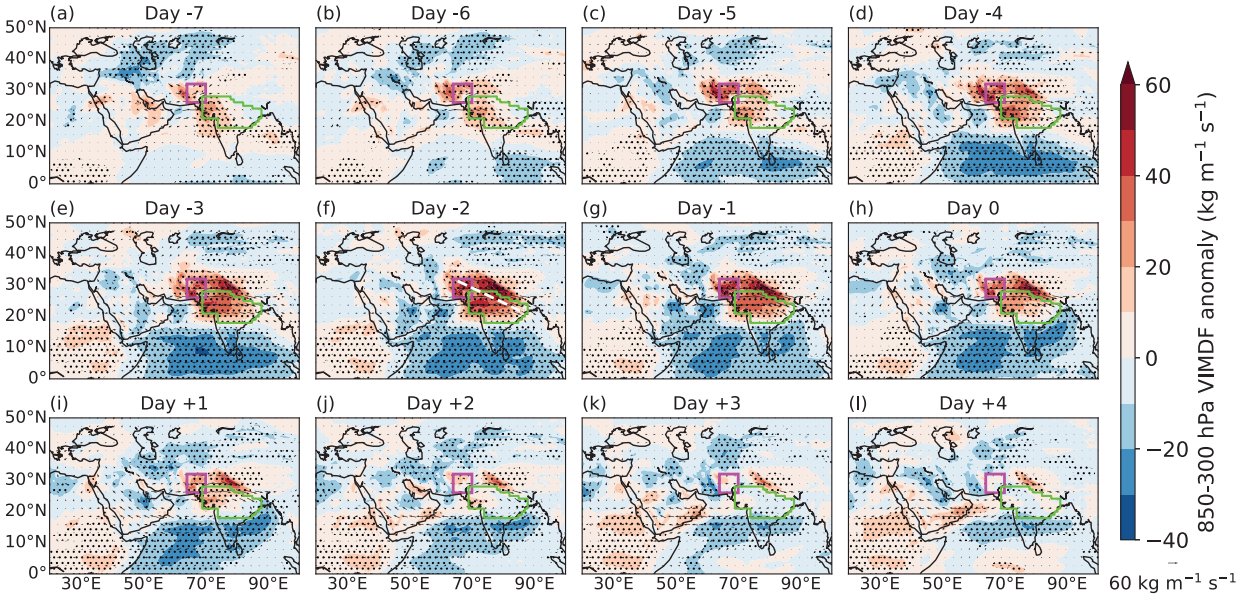

FIG. 3. Lead–lag composites of the 850–300-hPa VIMDF anomaly (kg m^{-1} s^{-1}) for 188 breaks during June–September 1940–2023. The anomaly is computed against a daily climatology during 1940–2023. Day 0 is the middle day of breaks. The core monsoon zone and northwest domain are highlighted in green and magenta, respectively, in each subplot. A white dashed line in (f) shows a transect used for computing vertical cross sections of equivalent potential temperature later in this study. Stippling denotes where the VIMDF anomaly is significantly different from zero at the 95% confidence level.

for which we follow the framework of Deoras et al. (2024). LAGRANTO uses a three-time iterative forward Euler scheme with an iteration step equal to 1/12 of the time spacing of the input data (i.e., 30 min for the 6-hourly ERA5 data considered for this analysis). As mentioned in section 2a, ERA5 is available at an hourly temporal resolution. However, the use of input data for the trajectories at a 6-hourly frequency is justified by previous relevant studies as it allows retention of the necessary accuracy in illustrating the synoptic-scale flow, while minimizing computing time (see Deoras et al. 2024 for an in-depth discussion).

Backward trajectories are computed by using the instantaneous three-dimensional wind field to calculate prior positions of the selected air parcels. For each break, trajectories are released at 0000 UTC on its middle day and are computed backward for 10 days. Trajectories are released at 600, 700, and 850 hPa from a region representative of the core monsoon zone (18°–26°N, 74°–85°E) with a release horizontal spacing of 0.25°, resulting in 108 starting locations for each of the three pressure levels. Thus, 324 trajectories are released in total for each break. As mentioned in section 2d, we are considering 188 breaks. This means that a total of 20 304 backward trajectories are released at each pressure level.

Trajectories are retained only if they pass through an additional box located to the northwest of the core monsoon zone (26°–32°N, 64°–70°E). This ensures that only the flow entering the core monsoon zone from the northwest is analyzed (see details in section 3a). While only around one in eight trajectories released at 850 hPa are retained (i.e., 2467 out of 20 304, ~12%), the number of retained trajectories increases for those released at 700 hPa (8983, ~44%) and 600 hPa (9245, ~46%).

As in Deoras et al. (2024), trajectories are stopped when leaving the horizontal domain of the input data (35°S–75°N, 15°–145°E) or when exceeding its upper boundary (200 hPa), and they reenter the atmosphere when hitting the ground. Relevant physical quantities, such as pressure and specific humidity and different flavors of potential temperature, are traced along the trajectories to examine variations in properties of the air mass flowing toward the core monsoon zone.

f. Significance testing

We use a Student's *t* test (Student 1908) to assess if anomalies are significantly different from zero. Our null hypothesis states that anomalies are not significantly different from zero. Thus, areas where anomalies are significantly different from zero at the 95% confidence level are stippled.

3. The relationship between dry intrusions and breaks

In this section, we examine the relationship between dry intrusions and breaks. We first investigate the origin of dry intrusions and then investigate how breaks evolve in response to dry intrusions. We then examine the relationship between the strength of dry intrusions and the frequency of breaks.

a. Lead–lag composites of dry intrusions

Figure 3 shows lead–lag composites of the VIMDF anomaly, calculated relative to the middle day of all breaks (i.e., day 0 in the figure). Dry air from arid regions to the west and northwest

of India starts entering the country 7 days prior to the middle day of breaks (Fig. 3a). On this day, the dry intrusion is strongest over southern Pakistan and nearby regions of western India (i.e., Gujarat and Rajasthan), where the VIMDF anomaly is 20–30 kg m^{-1} s^{-1}. Dry air is also present over the eastern Arabian Sea, in agreement with previous studies (e.g., Bhat 2006; Singh and Sandeep 2022, 2024). Five days prior to the middle day of breaks (Fig. 3c), the dry intrusion over Pakistan and nearby regions of Afghanistan strengthens, which is indicated by an increase in the VIMDF anomaly to ~50 kg m^{-1} s^{-1}; however, there is a smaller increase in the positive VIMDF anomaly over the core monsoon zone. Over subsequent days, the dry intrusion strengthens further and engulfs the core monsoon zone (Figs. 3d–g), attaining its peak strength over the Indo–Gangetic Plains 2–3 days prior to the middle day of breaks (Figs. 3e,f). The VIMDF anomalies over this region exceed 60 kg m^{-1} s^{-1} in this period. The dry intrusion starts weakening thereafter. In fact, VIMDF anomalies over the core monsoon zone and northern India on the middle day of breaks (Fig. 3h) are much smaller in magnitude than those observed 2–3 days prior to the middle day of breaks (i.e., Figs. 3e,f). By the fourth day after the middle day of breaks (Fig. 3l), the VIMDF anomaly over most of the core monsoon zone becomes positive, indicating the presence of anomalously moist air. The transport of dry air prior to the onset of breaks is, in general, in agreement with the findings of Prasanna and Annamalai (2012), who found that the horizontal advection of dry air into India acts as the initial trigger of breaks.

There is a region of cyclonic VIMDF anomaly to the southeast of the Caspian Sea around a week prior to the middle day of breaks (Fig. 3a), which weakens over subsequent days. Here, we speculate that its formation is either linked to midlatitude planetary wave activity (e.g., troughs embedded in the subtropical jet stream) or is a response to diabatic heating in the tropics (e.g., the diabatic heating associated with the MJO). Krishnan et al. (2000) have shown that an abrupt propagation of anomalous Rossby waves from the Bay of Bengal to northwest and central India triggers breaks, whereas Annamalai and Sperber (2005) have shown that enhanced convection over the tropical west Pacific forces Rossby waves, which in turn trigger monsoon breaks over central India. This perhaps suggests some combined role of the midlatitudes and tropics in triggering dry intrusions. However, examining this aspect is beyond the scope of this work.

We also analyze lead–lag composites of VIMDF anomalies for breaks identified using the ERA5 reanalysis (Fig. S2). On comparing Fig. S2 with Fig. 3, we do not find any noticeable difference, suggesting that our results are not sensitive to the choice of the dataset used for identifying breaks.

b. *Evolution of breaks in response to dry intrusions*

The results discussed in the previous subsection suggest that the dry intrusion starts entering northern and northwestern India around a week prior to the middle day of breaks. To better understand how breaks evolve in response to dry intrusions, we analyze the evolutions of the VIMDF anomaly over the northwest domain and precipitation over the core monsoon zone in this subsection.

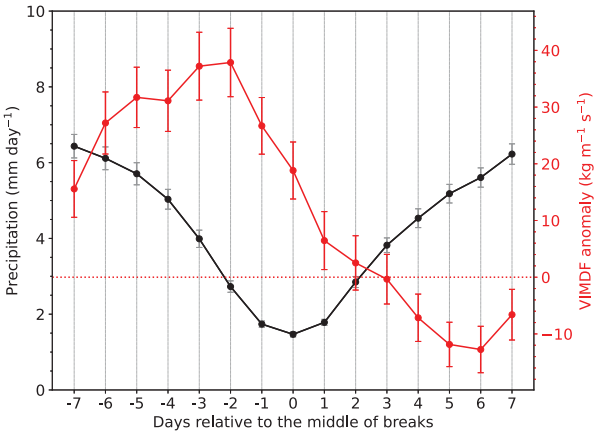

FIG. 4. Evolution of precipitation (solid black; mm day^{-1}) over the core monsoon zone and the VIMDF anomaly (kg m^{-1} s^{-1}) over the northwest domain (26°–32°N, 64°–70°E) for 850–300-hPa pressure levels (solid red). Day 0 is the middle day of breaks. The VIMDF anomaly is computed against a daily climatology over the years 1940–2023. Error bars show one standard error from the mean, and a horizontal dotted red line is used to show the VIMDF anomaly of 0 kg m^{-1} s^{-1}.

The positive VIMDF anomaly starts increasing from 7 days prior to the middle day of breaks (Fig. 4), which is consistent with the result discussed in the previous section (see Fig. 3a). At the same time, precipitation over the core monsoon zone starts decreasing. The dry intrusion over the northwest domain attains its peak strength 2–3 days prior to the middle day of breaks, and the mean VIMDF anomaly is approximately 40 kg m^{-1} s^{-1}. The core monsoon zone receives 4-mm precipitation on this day as the break begins. The dry intrusion starts weakening thereafter; however, precipitation continues to decrease until the middle day of breaks, when the core monsoon zone receives ~2-mm precipitation. Precipitation starts increasing thereafter, and a week after the middle day of breaks, its magnitude is comparable to that observed a week prior to the middle day of breaks. This result points toward two important aspects: First, there is a causal relationship between dry intrusions and breaks, and second, factors suppressing precipitation over the core monsoon zone do not recede immediately after the peak strength of dry intrusions is observed over north India. These aspects will be discussed later in this work.

c. *Relationship between the strength of dry intrusions and frequency of breaks*

Having analyzed the relationship between dry intrusions and breaks in the previous subsections, we now turn our attention to examining the relationship between the strength of dry intrusions over the northwest domain and the frequency of breaks. For each break, we calculate the standardized VIMDF anomaly over the northwest domain for a period between 7 days before and 7 days after the middle day of the break. For each day in this period, we then count the number of breaks preceded by a

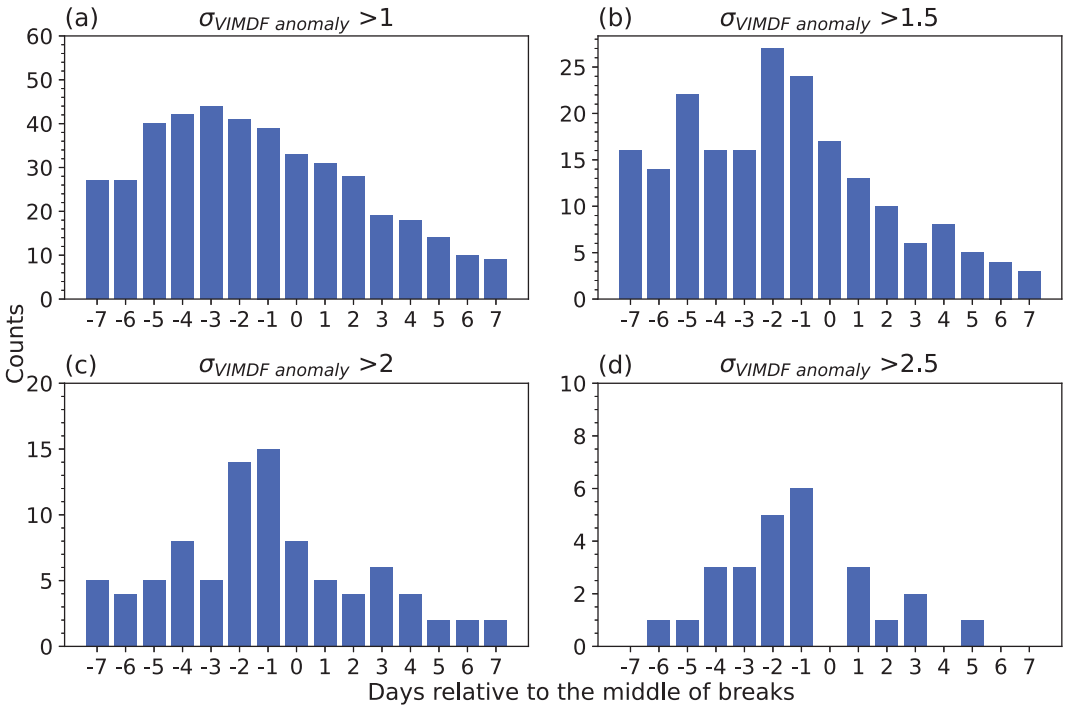

FIG. 5. Histograms showing counts of monsoon breaks associated with dry intrusions of various intensity. Standardized anomalies of 850–300-hPa VIMDF ($\sigma_{\text{VIMDF anomaly}}$) over the northwest domain (26°–32°N, 64°–70°E) are considered to determine the strength of dry intrusions. Day 0 is the middle day of breaks. Note the different *y*-axis interval in each subplot.

standardized VIMDF anomaly exceeding the following four thresholds: 1, 1.5, 2, and 2.5 standard deviations.

For the middle day of breaks, ~30 out of 188 (~16%) breaks are preceded by dry intrusions of standardized VIMDF anomaly greater than one (Fig. 5a). This fraction decreases as the intensity of dry intrusions increases. For example, only eight breaks are preceded by stronger dry intrusions featuring the standardized VIMDF anomaly greater than 2 (Fig. 5c). The frequency reduces further for even stronger dry intrusions (Fig. 5d). At all intensity thresholds, the frequency distribution is left skewed, which suggests the presence of a causal relationship between dry intrusions and breaks. Furthermore, the frequency of breaks for a large lag (e.g., 7 days prior to the middle day of breaks) is generally smaller than for a short lag (e.g., 2 days prior to the middle day of breaks). This suggests that dry intrusions associated with breaks intensify closer to the middle day of breaks, agreeing with the results discussed in previous subsections.

In summary, most breaks are associated with dry intrusions emanating from arid regions to the west and northwest of India. These dry intrusions start entering the country around a week prior to the middle day of breaks and attain their peak strength 2–3 days prior to the middle day of breaks. The frequency of breaks decreases as the strength of dry intrusions to the northwest of India increases.

4. Lagrangian analysis of dry intrusions

As discussed in section 1, Bhat (2006) and Krishnamurti et al. (2010) made use of Lagrangian trajectories for their analyses, revealing that the air from desert regions in West Asia traveled to India during breaks. However, those studies analyzed only a small number of breaks and computed only a few trajectories for each of those breaks. As mentioned in section 2e, we release three hundred twenty-four 10-day-long backward trajectories for each of the 188 breaks considered in this climatological study. In doing so, we can assess and generalize the validity of previous results, adding robustness and confidence to the results and providing a more detailed and quantitative analysis of the origin, path, and properties of the air flowing toward India during breaks. We release the trajectories from three pressure levels over the core monsoon zone (shown as a green rectangle in Figs. 6a–c) on the middle day of each break and, to isolate the air arriving from the northwest, we retain only those trajectories that pass through the northwest box (red square in Figs. 6a–c). Around one in eight trajectories released at 850 hPa and approximately half of those released at 700 and 600 hPa are retained (see more details in section 2e).

Figures 6a–c show the density of trajectory points for the trajectories released at the three pressure levels and passing through the northwest domain, with regions of high density highlighting preferred flow paths. Figure 6a shows that the most common path of the air arriving over the core monsoon zone at 850 hPa from the northwest is through the region located between 60° and 65°E and at around 35°N, to the west of the Hindu Kush and near the border between Afghanistan, Iran, and Turkmenistan. The density of trajectory points through this narrow gap between mountain ranges reaches 50% of the overall maximum. This is a particularly

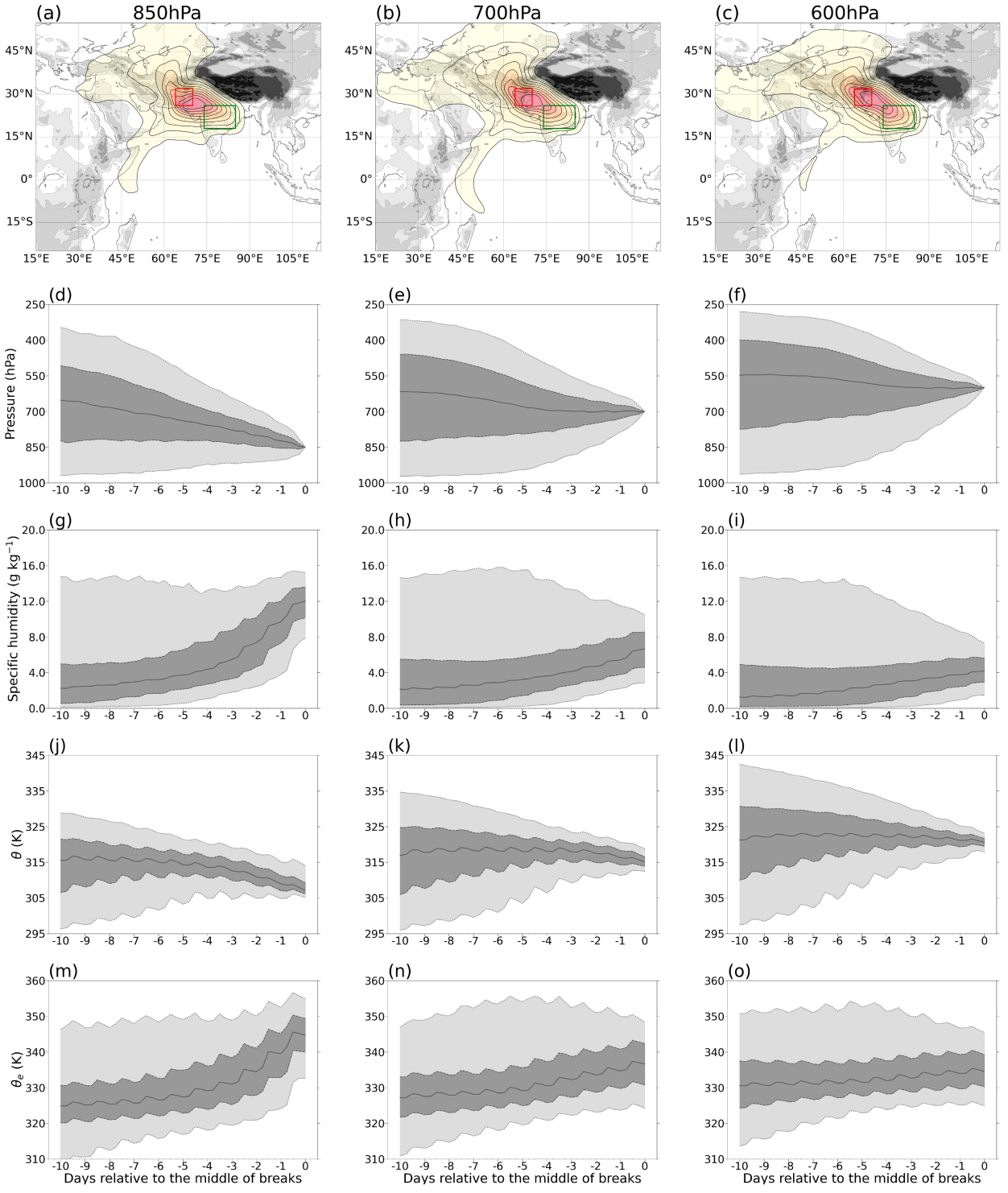

FIG. 6. Ten-day backward trajectories released at (a),(d),(g),(j),(m) 850, (b),(e),(h),(k),(n) 700, and (c),(f),(i),(l),(o) 600 hPa from the core monsoon zone [green rectangle in (a)] and passing through the northwest India domain [red box in (a)]. Trajectories are released at 0000 UTC on the middle day of 188 breaks during June–September 1940–2023. A kernel density estimate of trajectory points is shown for each case in (a)–(c), with gray-shaded orography. The time evolution of (d)–(f) pressure (hPa), (g)–(i) specific humidity (g kg^{-1}), (j)–(l) potential temperature (K), and (m)–(o) equivalent potential temperature (K) along trajectories starting at the above pressure levels is also shown. Solid black lines in these panels indicate the median of each field, dashed lines with dark gray shading between them indicate the 25th and 75th percentiles, and dotted lines with light gray shading between them indicate the 5th and 95th percentiles. Percentiles are calculated independently at each time; hence, a single percentile line can refer to different trajectories at different times.

clear indication that a large number of trajectories reach the core monsoon zone having originated in arid regions to the northwest of the Indian subcontinent, such as the central Asia plains, consistent with the 20% density contour extending north of the Pamir mountain range and crossing the Aral and Caspian Seas.

A secondary branch of the low-level flow crosses the Arabian Sea and enters the Indian subcontinent, flowing to the north of the Western Ghats between Gujarat and the Indus Valley. This branch follows the classic C-shaped Somali jet pattern (Findlater 1969), originating over the equatorial Indian Ocean and recurving over the western Arabian Sea as it flows over the Horn of Africa and then the southern coast of the Arabian Peninsula. A weak secondary maximum is also visible over the Persian Gulf, indicating that air flowing from the west, with the 10% contour extending as far as the eastern Mediterranean Sea, passes through this other terrain gap in its journey toward the northwest domain and the core monsoon zone.

It is worth reminding that, as explained in section 2e and repeated at the start of this section, in this study, we apply the constraint that trajectories have to pass through the northwest box, ensuring that we are only considering air arriving over the core monsoon zone from the northwest. This is why only eight trajectories released at 850 hPa are retained and shown here, while most of the trajectories belonging to the Somali jet, the dominant flow at low levels even during break events, are excluded from Fig. 6a (not shown). The purpose of this figure is indeed to highlight the presence and illustrate the path of the flow from arid regions, not part of the Somali jet flow that is typical of the monsoon season, particularly at low levels.

Figure 6b shows the density of trajectory points for the trajectories released over the core monsoon zone at 700 hPa and passing through the northwest box; 700 hPa is a pressure level where the intrusion of dry air is more commonly observed, as shown for the monsoon onset and withdrawal, respectively, in Parker et al. (2016) and Deoras et al. (2024). Almost half of the trajectories released at 700 hPa pass through the northwest box and are thus retained. This is roughly 4 times the proportion of those released at 850 hPa, highlighting the increased importance of northwesterly flow arriving in the monsoon core zone at 700 hPa. The most common path for these trajectories is, like for those released at 850 hPa, from West and central Asia and through the terrain gap to the west of the Hindu Kush. The Aral and Caspian Seas in this case are reached by the 30% density contour, while the 10% contour extends west all the way to the central Mediterranean Sea, highlighting the remote origin and westerly component of a nonnegligible part of the flow toward the monsoon region. The Somali jet branch is still present, but as in Fig. 6a, the 20% contour does not extend far over the Arabian Sea, stopping well before the Horn of Africa and highlighting the secondary role of this flow.

Focusing on air arriving at the core monsoon zone at 600 hPa (Fig. 6c), where slightly less than half of the released trajectories pass through the northwest box and are therefore retained, the westerly branch of the flow becomes even more dominant and the Somali jet branch even more secondary. Maximum density values are oriented along a southeast-to-northwest direction over northwest India, Pakistan, and the mountain ranges to their northwest, where they become approximately zonal, with the 30% contour extending all the way to Iraq and the 20% contour reaching Egypt. The influence of terrain gaps is less obvious for these trajectories, traveling at higher levels than those in Figs. 6a and 6b. Overall, these maps indicate that trajectories released over the core monsoon zone and passing over north India at pressure levels typical of dry air intrusions are likely to have remote origins and to have flown mainly zonally for thousands of kilometers over arid regions in West and central Asia.

Time series of quantities traced along the trajectories are shown in Figs. 6d–o, illustrating processes taking place as the air flows toward the core monsoon zone and passes through the northwest domain. Air arriving at the core monsoon zone at 850 hPa experiences a steady descent from around 650 hPa over the course of 10 days (Fig. 6d). At the same time, specific humidity increases, initially slowly and considerably more quickly in the last 3 days, with the median value going from around 2 g kg^{-1} to well above 12 g kg^{-1} (Fig. 6f). Ignoring oscillations from the diurnal cycle, potential temperature θ is roughly constant over the first 5 days and then decreases by nearly 10 K in the following 5 days (Fig. 6j). Equivalent potential temperature θ_e markedly increases, from below 330 K to around 345 K, in the last 4 days (Fig. 6m). This behavior indicates that the initially dry midtropospheric air descends gradually toward 850 hPa and moistens rapidly in the second part of its descent as it moves toward the monsoon region and starts interacting with the moister environment and the Somali jet flow. The associated evaporative cooling causes a decrease in θ and is only partially balanced by mixing with air belonging to the warmer environment over the Arabian Sea, which increases θ_e.

The properties of trajectories released over the core monsoon zone at 700 hPa are noticeably different. Their descent is more limited (Fig. 6e), and the marked changes in specific humidity, θ, and θ_e characterizing the trajectories released at 850 hPa are in this case absent. In detail, the median of specific humidity stays well below 8 g kg^{-1} (Fig. 6h), median variations in θ do not exceed 5 K (Fig. 6k), and the increase in θ_e is now steady and overall roughly halved to around 10 K (Fig. 6n). Similar behavior is observed for trajectories released at 600 hPa, but with even more limited descent (Fig. 6f), increases in specific humidity (Fig. 6i) and θ_e (Fig. 6o), and changes in θ (Fig. 6l).

To summarize, Lagrangian backward trajectories show that the flow from arid regions in West and central Asia, and even from remote regions such as the Mediterranean, constitutes an integral component of the air arriving at the core monsoon zone from the northwest on the middle day of breaks. The most common path for these trajectories, particularly for those arriving in the lower troposphere, passes through the terrain gap to the west of the Hindu Kush range and near the border between Afghanistan, Iran, and Turkmenistan. This behavior is consistent with the results in Boos and Hurley (2013), which highlighted the advection of dry air through regions of reduced terrain height to the west of the Himalaya and Hindu Kush. Examining the time evolution of physical quantities along these trajectories, we see that the

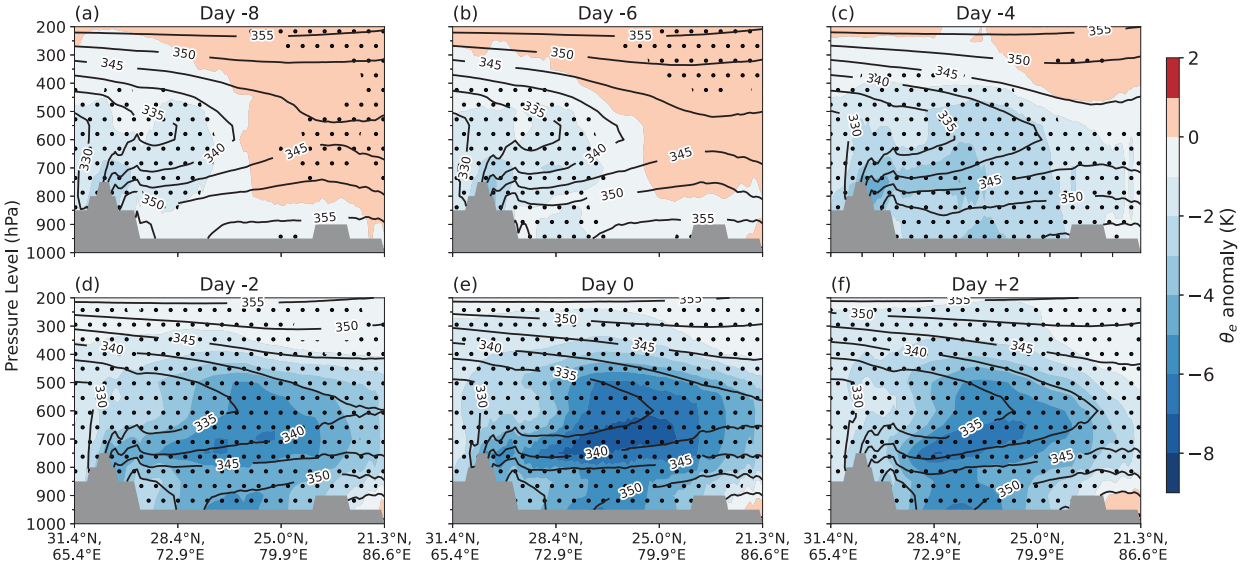

FIG. 7. Lead–lag composites of the northwest-to-southeast cross section of equivalent potential temperature (K; line contours) and equivalent potential temperature anomaly (K; shading) for 188 monsoon breaks during June–September 1940–2023. The anomaly is computed against a daily climatology over the years 1940–2023. Day 0 is the middle day of breaks. Gray areas show the orography, and stippling denotes where the equivalent potential temperature anomaly is significantly different from zero at the 95% confidence level.

low-level flow is characterized by rapid moistening and mixing of the dry air flowing from arid regions, as it starts interacting with warmer air over the Arabian Sea. These processes are much more limited for the trajectories that are still in the midtroposphere when they reach the monsoon core zone. The results of this section thus confirm the primary importance of dry air intrusions in breaks, highlighting their remote origin and westerly or northwesterly flow over arid regions.

5. Thermodynamics of dry intrusions

In previous sections, we discussed how breaks are related to dry intrusions, so we attempt to understand how dry intrusions alter the atmospheric thermodynamics and help support monsoon breaks. In this section, we analyze vertical cross sections of θ_e, which will help assess the static stability in the troposphere.

a. Vertical cross sections of θ_e along a transect

Parker et al. (2016) and Deoras et al. (2024) analyzed vertical cross sections of θ_e along a northwest-to-southeast transect over India to understand the role of dry intrusions in progressions of the onset and withdrawal, respectively. We follow their framework for analyzing lead–lag composites of vertical cross sections of θ_e in this subsection. We consider a transect shown in Fig. 1a, whose position differs slightly from that considered by Parker et al. (2016) and Deoras et al. (2024). While both transects initiate near Kandahar (southeastern Afghanistan), the transect considered in this study terminates near Balasore (eastern India) as opposed to near Vizag (southeastern India) in Parker et al. (2016) and Deoras et al. (2024). This is because the dry air that causes breaks is more prevalent over eastern India than over southeastern India (see Fig. 3f for example).

Eight days prior to the middle day of breaks, the dry air is already present over parts of Afghanistan, Pakistan, and northwest India at midlevels (Fig. 7a). The θ_e near 600 hPa is ~335 K, and its anomaly is −3 K. In comparison, θ_e at other places along the transect (e.g., eastern India) and at lower levels (e.g., 800 hPa) is larger. This suggests that these dry intrusions are of midlevel origin, similar to those modulating progressions of the onset and withdrawal of the monsoon (Parker et al. 2016; Deoras et al. 2024).[2] Over subsequent days, the midlevel dry intrusion expands to the southeast and descends, reducing the θ_e in the mid- and lower troposphere. Two days prior to the middle day of breaks, the midlevel θ_e over eastern India reduces to ~340 K, and the θ_e anomaly is around −5 K (Fig. 7d). The θ_e anomaly along the transect is strongest on the middle day of breaks (Fig. 7e) and has a magnitude of −8 K at ~700 hPa over north-central India (i.e., near 25°N, 80°E). At midlevels, the magnitude of θ_e reduces to ~335 K over this region when compared with ~345 K 8 days prior to the middle day of breaks, whereas the θ_e anomaly reduces from 1 to −7 K. While the dry intrusion starts weakening 2 days after the middle day of breaks (Fig. 7f), the magnitude of the midlevel θ_e over northwest India continues to remain around 335 K. Singh and Sandeep (2022) analyzed the vertical structure of the θ_e anomaly over a nearby

[2] In order to test if there is any contamination of the results by the onset progression and withdrawal of the monsoon, we analysed the absolute and anomalous θ_e along the transect for 105 breaks whose middle days occurred during July and August. We did not find any noticeable difference, confirming that dry intrusions modulating breaks are similar to those modulating progressions of the onset and withdrawal of the monsoon.

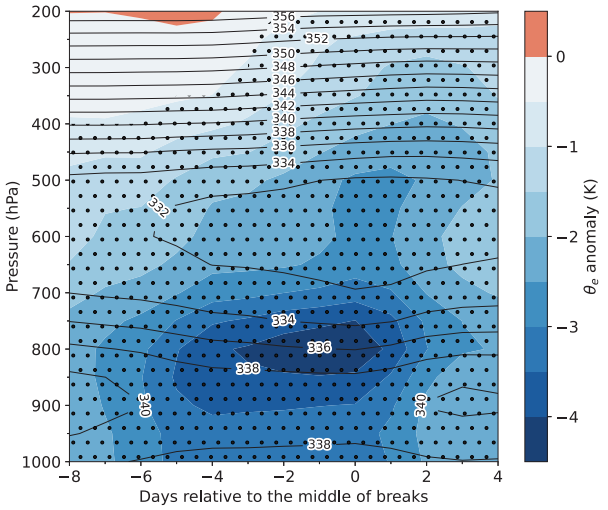

FIG. 8. Time–pressure section of equivalent potential temperature (K; line contours) and equivalent potential temperature θ_e anomaly (K; shading) over the northwest domain (26°–32°N, 64°–70°E) for 188 breaks during June–September 1940–2023. The anomaly is computed against a daily climatology over the years 1940–2023. Day 0 is the middle day of breaks. Stippling denotes where the θ_e anomaly is significantly different from zero at the 95% confidence level.

region in northwest India (20°–30°N, 65°–75°E) during dry intrusion events. They found the largest θ_e anomaly of about −7 K between 850 and 700 hPa, which generally agrees with our result.

A magnitude of θ_e exceeding ~350 K is normally sufficient to support deep convection in the tropics (Bhat 2006). As the midlevel dry intrusion expands southeastward prior to the middle day of breaks, θ_e decreases below 350 K, indicating an unfavorable environment for deep convection. Deoras et al. (2024) found that the low-level θ_e decreases as the midlevel dry intrusion expands to the southeast during the monsoon withdrawal, which tends to increase convective inhibition (CIN) and decrease convective available potential energy. Midlevel dry intrusions cap the moist boundary layer, decreasing the buoyancy of boundary layer parcels and increasing CIN (Aslam et al. 2024). Here, we expect a similar thermodynamic scenario, in which an increase in the static stability in the troposphere suppresses deep convection, agreeing with the findings of Prasanna and Annamalai (2012).

b. *Evolution of θ_e over the northwest domain*

After analyzing θ_e along the transect, we now carry out a closer inspection of its temporal evolution during breaks. Figure 8 shows the evolution of the vertical structure of θ_e and its anomaly for the northwest domain, composited between 8 days prior to and 4 days after the middle day of breaks. Eight days prior to the middle day of breaks, the θ_e anomaly in most of the mid- and lower troposphere is negative. About 6 days prior to the middle day of breaks, the θ_e anomaly at midlevels is about −2 K, and θ_e reduces to 332 K. At lower levels, the θ_e anomaly reduces to −3 K. About 3 days prior, the largest θ_e anomaly of about −4 K occurs in low levels, whereas anomalies at midlevels are relatively weaker. Over subsequent days, the dry intrusion descends into lower levels, which is indicated by a decrease in θ_e and an increase in θ_e anomalies. The presence of the dry air continues after the middle day of breaks, indicating an unfavorable environment for deep convection. Over subsequent days, the impact of dry air weakens gradually, which can be inferred from a gradual increase in the magnitude of θ_e and a reduction in θ_e anomalies.

In summary, dry intrusions causing breaks are of midlevel origin, similar to those driving the monsoon withdrawal. They are first observed over arid regions to the west and northwest of India around a week prior to the middle day of breaks. They expand southeastward and descend, increasing the static stability in the troposphere and suppressing deep convection.

6. The role of dry intrusions in the duration of breaks

Having analyzed the thermodynamics of dry intrusions in the previous section, we now analyze the relationship between the strength of dry intrusions and the duration of breaks. This will help understand if stronger dry intrusions are responsible for prolonging breaks, which has not been investigated previously. For each break, we first consider a period between its onset and the middle day and then calculate the maximum VIMDF anomaly over the northwest domain. The choice of this time period will ensure that we test the causal relationship between the strength of dry intrusions and the duration of breaks. As discussed in section 2d, the mean duration of breaks is 5.5 days. Most breaks feature a duration of 3–4 days (see Fig. 2c) and are associated with a median and mean maximum VIMDF anomaly of ~15 kg m^{-1} s^{-1} (Fig. 9). There is a considerable increase in the mean maximum intensity of dry intrusions associated with breaks featuring a duration of at least 6 days. Breaks lasting 6 days are associated with a median maximum VIMDF anomaly of ~125 kg m^{-1} s^{-1}. The sample size of very long breaks (e.g., breaks longer than 11 days; see Fig. 2c) is mostly small, making it difficult to draw conclusions. However, the mean maximum VIMDF anomaly associated with such breaks is larger than that associated with short duration breaks.

We now focus on understanding the evolution of precipitation over the core monsoon zone and dry air over the northwest domain for short and extended breaks. We define short and extended breaks as those lasting for 3 days and at least 7 days, respectively. This gives us 56 short and 54 extended breaks, with both categories containing roughly 30% of the total number of breaks (188). The core monsoon zone receives significantly less rainfall on the middle day of extended breaks compared to short breaks, with precipitation remaining below 2 mm day^{-1} for a longer duration (Fig. 10). For extended breaks, the dry intrusion attains its peak strength 3–5 days prior to the middle day of breaks, whereas for short breaks, it attains its peak strength on the middle day of breaks. While the peak VIMDF anomaly for short breaks is ~25 kg m^{-1} s^{-1}, that for extended breaks is ~55 kg m^{-1} s^{-1}. The positive VIMDF anomaly for extended breaks increases from ~12 days prior to the middle day, whereas for short breaks, positive anomalies steadily increase from 7 days prior to the middle day of breaks.

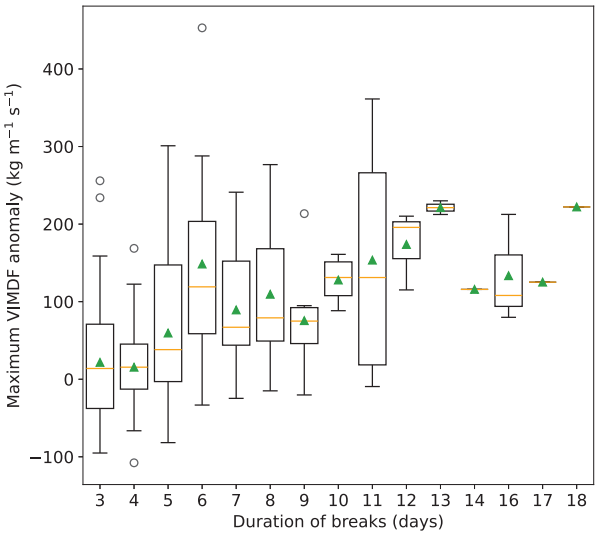

FIG. 9. Box-and-whisker plot showing the relationship between the maximum 850–300-hPa VIMDF anomaly over the northwest domain (26°–32°N, 64°–70°E) and the duration of 188 monsoon breaks during June–September 1940–2023. Orange lines, green triangles, and black diamonds show the median VIMDF anomaly, mean VIMDF anomaly, and outliers, respectively. For each break, the occurrence of the maximum VIMDF anomaly is identified over a period between the onset and the middle day of the break to test causality.

In summary, the strength of dry intrusions over the northwest domain modulates the duration of breaks, with strong dry intrusions acting as precursors of extended breaks.

7. Conclusions

The Indian summer monsoon (hereafter the monsoon) is crucial to over a billion people since it contributes over 75% of India's annual precipitation. Intraseasonal variability in monsoon rainfall directly impacts the rain-dependent agricultural sector and other users of water resources, with breaks in rainfall often triggering droughts that can have a significant economic impact. Previous studies have shown that dry intrusions are observed during breaks; however, the role they play in causing breaks is less understood compared to that played during progressions of the onset and withdrawal of the monsoon. In this study, we used the ERA5 reanalysis to understand the role of dry intrusions in breaks. We developed an index to measure the moisture-deficit flux in the troposphere and identified 188 breaks using the India Meteorological Department's gridded precipitation dataset for the period June–September 1940–2023. The key findings of our study are summarized as follows:

- Around a week prior to the middle day of breaks, the dry air from arid regions west and northwest of India starts entering the country, and precipitation over the core monsoon zone (i.e., central India) starts decreasing.
- A thermodynamic analysis reveals that this dry intrusion is of midlevel origin, similar to that driving the withdrawal of the monsoon (Deoras et al. 2024).
- Over subsequent days, the dry intrusion intensifies, expands southeastward, and descends. It attains its peak intensity over northwest India and adjoining eastern Pakistan 2–3 days prior to the middle day of breaks. This increases the tropospheric stability, causing a further decrease in precipitation over the core monsoon zone.
- By the middle day of breaks, the core monsoon zone and north India are engulfed in the dry air. The core monsoon zone receives the least precipitation on the middle day of breaks.
- Backward trajectories released over the core monsoon zone and flowing from the northwest are most likely to originate in remote arid regions and reach the monsoon region by flowing through terrain gaps, and in particular through the

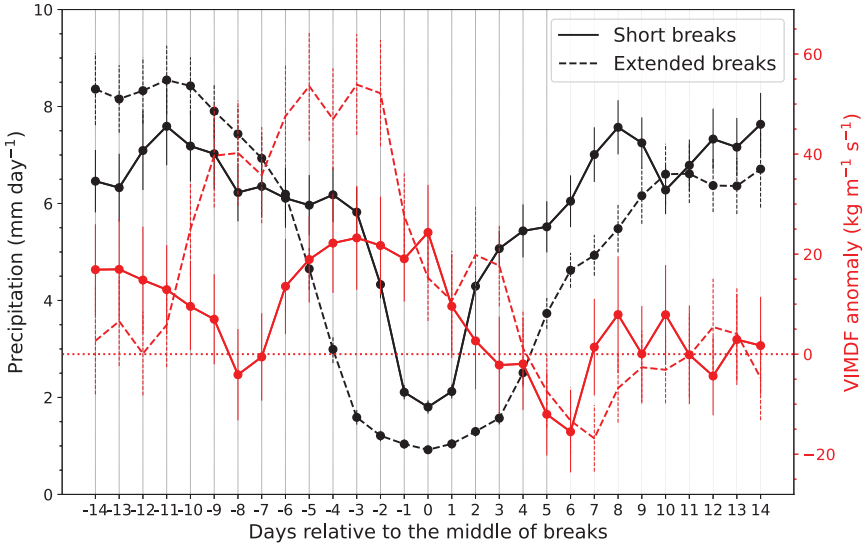

FIG. 10. As in Fig. 4, but showing the results for 56 short and 54 extended breaks. Note that the result is shown for a period between 14 days before and after the middle day of breaks.

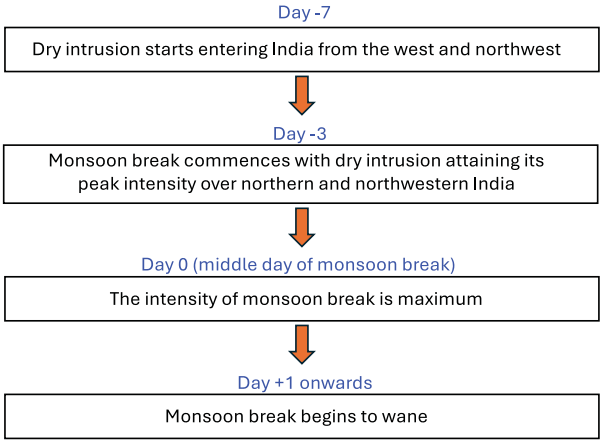

FIG. 11. Schematic diagram encapsulating the causal relationship between dry intrusions and breaks.

region to the west of the Hindu Kush and near the border between Afghanistan, Iran, and Turkmenistan.

- These results corroborate and expand those of previous studies (Bhat 2006; Krishnamurti et al. 2010), with our analysis of a larger sample of trajectories and break events revealing that trajectories reaching the core zone at low levels moisten rapidly when they eventually interact with the monsoon flow arriving from the Arabian Sea, while those staying at midlevels remain dry.
- The impact of the dry intrusion weakens gradually in the days following the middle day of breaks, and precipitation over the core monsoon zone increases.
- Strong dry intrusions increase the duration of breaks, whereas the frequency of breaks decreases as the strength of dry intrusions increases.

The results of this study help establish a causal relationship between midlevel dry intrusions and breaks, which is illustrated schematically in Fig. 11. This could help design new forecasting products for breaks, which could ultimately benefit stakeholders (e.g., farmers and water resources managers) in improving long-term planning in India.

A limitation of this study is that we did not investigate large-scale drivers of dry intrusions. This includes the examination of factors behind the anomalous cyclonic flux of dry air, which is present to the southeast of the Caspian Sea around a week prior to the middle day of breaks. In a future study, researchers could examine the role of the midlatitudes and tropics in triggering the anomalous cyclonic flux of dry air. They could perform sensitivity experiments by imposing diabatic heating over the tropical Indian Ocean at different lag times and examine if it triggers midlatitude dry intrusions. This will help understand if midlatitude circulation patterns responsible for triggering dry intrusions are independent, or themselves excited by the tropics. As discussed in section 1, modes of tropical intraseasonal variability modulate breaks; however, their scale interactions with dry intrusions remain unexplored. Researchers could use the catalogue of dry intrusions developed in this study to examine these scale interactions, which could help connect regional and global scales with dry intrusions and breaks. The predictability of dry intrusions needs to be explored in a future study since that would immensely benefit stakeholders in India.

Acknowledgments. All authors are funded through the Weather and Climate Science for Service Partnership (WCSSP) India project (OUTBREAK), a collaborative initiative between the Met Office, supported by the U.K. Department for Science, Innovation, and Technology (DSIT), and the Indian Ministry of Earth Sciences (MoES). AD, AGT, and AV are also supported by the Natural Environment Research Council (MiLCMOP project; Grant: NE/X000176/1).

Data availability statement. The ERA5 hourly data on pressure levels are available at https://doi.org/10.24381/cds.bd0915c6. The IMD's high-resolution daily gridded precipitation dataset is available at https://www.imdpune.gov.in/cmpg/Griddata/Rainfall_25_NetCDF.html. The Python interface for LAGRANTO, which provides scripts used for the trajectory calculations in this article, is available at https://github.com/leosaffin/pylagranto. The mask for the core monsoon zone was digitized from Fig. 4a of Rajeevan et al. (2010) using the WebPlotDigitizer software (https://automeris.io/WebPlotDigitizer).

REFERENCES

Annamalai, H., and K. R. Sperber, 2005: Regional heat sources and the active and break phases of boreal summer intraseasonal (30–50 day) variability. *J. Atmos. Sci.*, **62**, 2726–2748, https://doi.org/10.1175/JAS3504.1.

Aslam, A. A., J. Schwendike, S. C. Peatman, C. E. Birch, M. A. Bollasina, and P. Barrett, 2024: Mid-level dry air intrusions over the southern Maritime Continent. *Quart. J. Roy. Meteor. Soc.*, **150**, 727–745, https://doi.org/10.1002/qj.4618.

Bhat, G. S., 2006: The Indian drought of 2002—A sub-seasonal phenomenon? *Quart. J. Roy. Meteor. Soc.*, **132**, 2583–2602, https://doi.org/10.1256/qj.05.13.

Bhatla, R., U. C. Mohanty, P. V. S. Raju, and O. P. Madan, 2004: A study on dynamic and thermodynamic aspects of breaks in the summer monsoon over India. *Int. J. Climatol.*, **24**, 341–360, https://doi.org/10.1002/joc.1005.

Blanford, H. F., 1886: *The Rainfall of India.* Superintendent Government Print, 658 pp.

Boos, W. R., and J. V. Hurley, 2013: Thermodynamic bias in the multimodel mean boreal summer monsoon. *J. Climate*, **26**, 2279–2287, https://doi.org/10.1175/JCLI-D-12-00493.1.

Chuphal, D. S., A. P. Kushwaha, S. Aadhar, and V. Mishra, 2024: Drought atlas of India, 1901–2020. *Sci. Data*, **11**, 7, https://doi.org/10.1038/s41597-023-02856-y.

De, U. S., and R. K. Mukhopadhyay, 2002: Breaks in monsoon and related precursors. *Mausam*, **53**, 309–318, https://doi.org/10.54302/mausam.v53i3.1647.

Deoras, A., A. G. Turner, A. Volonté, and A. Menon, 2024: The role of midlatitude dry air during the withdrawal of the Indian summer monsoon. *Quart. J. Roy. Meteor. Soc.*, **150**, 5094–5112, https://doi.org/10.1002/qj.4859.

Findlater, J., 1969: A major low-level air current near the Indian Ocean during the northern summer. *Quart. J. Roy. Meteor. Soc.*, **95**, 362–380, https://doi.org/10.1002/qj.49709540409.

Gadgil, S., 2006: The Indian monsoon. *Resonance*, **11**, 8–21, https://doi.org/10.1007/bf02834470.

——, and P. V. Joseph, 2003: On breaks of the Indian monsoon. *J. Earth Syst. Sci.*, **112**, 529–558, https://doi.org/10.1007/BF02709778.

Hersbach, H., 2023: ERA5 reanalysis now available from 1940. ECMWF Newsletter, No. 175, ECMWF, Reading, United Kingdom, https://www.ecmwf.int/en/newsletter/175/news/era5-reanalysis-now-available-1940.

——, and Coauthors, 2020: The ERA5 global reanalysis. *Quart. J. Roy. Meteor. Soc.*, **146**, 1999–2049, https://doi.org/10.1002/qj.3803.

Joseph, P. V., and S. Sijikumar, 2004: Intraseasonal variability of the low-level jet stream of the Asian summer monsoon. *J. Climate*, **17**, 1449–1458, https://doi.org/10.1175/1520-0442(2004)017<1449:IVOTLJ>2.0.CO;2.

Kikuchi, K., 2021: The boreal summer intraseasonal oscillation (BSISO): A review. *J. Meteor. Soc. Japan*, **99**, 933–972, https://doi.org/10.2151/jmsj.2021-045.

Krishnamurti, T. N., A. Thomas, A. Simon, and V. Kumar, 2010: Desert air incursions, an overlooked aspect, for the dry spells of the Indian summer monsoon. *J. Atmos. Sci.*, **67**, 3423–3441, https://doi.org/10.1175/2010JAS3440.1.

Krishnan, R., C. Zhang, and M. Sugi, 2000: Dynamics of breaks in the Indian summer monsoon. *J. Atmos. Sci.*, **57**, 1354–1372, https://doi.org/10.1175/1520-0469(2000)057<1354:DOBITI>2.0.CO;2.

Mahto, S. S., and V. Mishra, 2019: Does ERA-5 outperform other reanalysis products for hydrologic applications in India? *J. Geophys. Res. Atmos.*, **124**, 9423–9441, https://doi.org/10.1029/2019JD031155.

Pai, D. S., J. Bhate, O. P. Sreejith, and H. R. Hatwar, 2011: Impact of MJO on the intraseasonal variation of summer monsoon rainfall over India. *Climate Dyn.*, **36**, 41–55, https://doi.org/10.1007/s00382-009-0634-4.

——, M. Rajeevan, O. P. Sreejith, B. Mukhopadhyay, and N. S. Satbha, 2014: Development of a new high spatial resolution (0.25° × 0.25°) long period (1901-2010) daily gridded rainfall data set over India and its comparison with existing data sets over the region. *MAUSAM*, **65**(1), 1–18, https://doi.org/10.54302/mausam.v65i1.851.

——, L. Sridhar, and M. R. Ramesh Kumar, 2016: Active and break events of Indian summer monsoon during 1901–2014. *Climate Dyn.*, **46**, 3921–3939, https://doi.org/10.1007/s00382-015-2813-9.

Parker, D. J., P. Willetts, C. Birch, A. G. Turner, J. H. Marsham, C. M. Taylor, S. Kolusu, and G. M. Martin, 2016: The interaction of moist convection and mid-level dry air in the advance of the onset of the Indian monsoon. *Quart. J. Roy. Meteor. Soc.*, **142**, 2256–2272, https://doi.org/10.1002/qj.2815.

Parthasarathy, B., and D. A. Mooley, 1978: Some features of a long homogeneous series of Indian summer monsoon rainfall. *Mon. Wea. Rev.*, **106**, 771–781, https://doi.org/10.1175/1520-0493(1978)106<0771:SFOALH>2.0.CO;2.

Pisharoty, P, and G. Asnani, 1960: Flow pattern over India and neighbourhood at 500 mb during the monsoon. *Proc. Symp on Monsoons of the World*, New Delhi, India, The Hind Union Press, 112–117.

Prasanna, V., and H. Annamalai, 2012: Moist dynamics of extended monsoon breaks over South Asia. *J. Climate*, **25**, 3810–3831, https://doi.org/10.1175/JCLI-D-11-00459.1.

Raghavan, K., 1973: Break-monsoon over India. *Mon. Wea. Rev.*, **101**, 33–43, https://doi.org/10.1175/1520-0493(1973)101<0033:BOI>2.3.CO;2.

Rai, D., and S. Raveh-Rubin, 2023: Enhancement of Indian summer monsoon rainfall by cross-equatorial dry intrusions. *npj Climate Atmos. Sci.*, **6**, 43, https://doi.org/10.1038/s41612-023-00374-7.

Rajeevan, M., S. Gadgil, and J. Bhate, 2010: Active and break spells of the Indian summer monsoon. *J. Earth Syst. Sci.*, **119**, 229–247, https://doi.org/10.1007/s12040-010-0019-4.

Ramamurthy, K., 1969: Monsoon of India: Some aspects of the 'break' in the Indian southwest monsoon during July and August. India Meteorological Department FMU Rep. IV-1813, 57 pp.

Ramaswamy, C., 1962: Breaks in the Indian summer monsoon as a phenomenon of interaction between the easterly and the sub-tropical westerly jet streams. *Tellus*, **14**, 337–349, https://doi.org/10.3402/tellusa.v14i3.9560.

Rao, Y., 1976: *Southwest Monsoon*. *Synoptic Meteorology*, *Meteor. Monogr.*, Vol. 1, India Meteorological Department, 376 pp.

Rodwell, M. J., 1997: Breaks in the Asian monsoon: The influence of Southern Hemisphere weather systems. *J. Atmos. Sci.*, **54**, 2597–2611, https://doi.org/10.1175/1520-0469(1997)054<2597:BITAMT>2.0.CO;2.

Samanta, D., M. K. Dash, B. N. Goswami, and P. C. Pandey, 2016: Extratropical anticyclonic Rossby wave breaking and Indian summer monsoon failure. *Climate Dyn.*, **46**, 1547–1562, https://doi.org/10.1007/s00382-015-2661-7.

Shepard, D., 1968: A two-dimensional interpolation function for irregularly-spaced data. *Proceedings of the 1968 23rd ACM National Conference*, Association for Computing Machinery, 517–524, https://doi.org/10.1145/800186.810616.

Singh, R., and S. Sandeep, 2022: Dynamics of dry air intrusion over India during summer monsoon breaks. *Climate Dyn.*, **59**, 1649–1664, https://doi.org/10.1007/s00382-021-06060-9.

——, and ——, 2024: A mechanism for the summer monsoon precipitation variability over northwest India driven by moisture deficit transport. *J. Geophys. Res. Atmos.*, **129**, e2023JD040180, https://doi.org/10.1029/2023JD040180.

Sprenger, M., and H. Wernli, 2015: The LAGRANTO Lagrangian analysis tool—Version 2.0. *Geosci. Model Dev.*, **8**, 2569–2586, https://doi.org/10.5194/gmd-8-2569-2015.

Student, 1908: The probable error of a mean. *Biometrika*, **6**(1), 1–25, https://doi.org/10.2307/2331554.

Wang, B., and X. Xie, 1997: A model for the boreal summer intraseasonal oscillation. *J. Atmos. Sci.*, **54**, 72–86, https://doi.org/10.1175/1520-0469(1997)054<0072:AMFTBS>2.0.CO;2.